Time-Dependent Propagation Analysis and Modeling of LPWAN Technologies

Martin Stusek[1,2], Dmitri Moltchanov[2], Pavel Masek[1], Sergey Andreev[2], Yevgeni Koucheryavy[2], and Jiri Hosek[1]
[1]Department of Telecommunications, Brno University of Technology, Brno, Czech Republic
[2]Unit of Electrical Engineering, Tampere University, Finland
✉Contact author's e-mail: masekpavel@vutbr.cz

***Abstract*—Contemporary low-power wide area network (LPWAN) technologies have been introduced as connectivity enablers with low complexity, extended communication range, and excellent signal penetration. On the other hand, they suffer from a substantial delay and low packet-delivery guarantees. As a result, numerous novel applications entering the Internet of things (IoT) market suffer from insufficient performance. To mitigate this issue, further optimization and adaptation of the LPWAN technologies to the needs of these new applications requires an in-depth understanding of the propagation environment dynamics. Motivated by that, in this paper, we thoroughly investigate time-dependent statistical characteristics of the reference signal receive power (RSRP) dynamics of Narrowband IoT (NB-IoT) technology. We demonstrate that even for a stationary user equipment, RSRP is subject to drastic variations that are characterized by exponentially decaying autocorrelation function. We then demonstrate that first- and second-order statistical properties of the RSRP dynamics can be closely captured using a doubly-stochastic Markov model that retains the tractability of the conventional Markov models. The reported model is expected to serve as a building block for analytical and simulation-based system-level studies and optimization of LPWAN technologies.**

***Index Terms*—Propagation modeling; time-dependent propagation characteristics; LPWAN; NB-IoT; Markov model**

I. Introduction

The machine-type communication (MTC) can be divided into two broad categories [1]. The first one aims at applications having no strict delay and loss requirements, but which are characterized by extreme densities of user equipments (UEs). These applications are classified as massive MTC (mMTC) and nowadays they are supported by low-power wide-area networks (LPWANs), such as Narrowband IoT (NB-IoT), LoRaWAN, and Sigfox. These LPWANs have been developed having M.2412 service requirements in mind [2]. Based on the above, at least 90 % of messages have to be delivered over the radio interface in less than 10 s. Another service category, named ultra-reliable low-latency communication (URLLC), poses extreme latency requirements at the air interface, e.g., under 5 ms one-way delay [1]. The third generation partnership project (3GPP) is currently standardizing the radio access technologies (RATs) that are expected to support this service as part of the New Radio (NR) interface [3].

At the same time, numerous emerging MTC applications fall in-between these two extremes, e.g., presence monitoring, industrial asset tracking, condition-based monitoring, patient monitoring. These applications pose much stricter requirements on delay and loss performance compared to mMTC, but they, however, remain much more relaxed than the ones given by URLLC. They are also characterized by comparable deployment densities to those supported by LPWANs [1]. Furthermore, the reliability and availability of these applications are becoming much more critical as opposed to power consumption since constant power supply might be available. As a result, the delay is becoming a deciding factor in selecting URLLC vs. mMTC connectivity enablers [1].

There are two possible ways of addressing the needs of these novel uncategorized applications within the MTC landscape. The first approach suggests developing a specific RAT supporting these applications, e.g., DECT-2020 mMTC initiative [3]. On the other hand, one may adapt and extend the existing LPWAN solutions to improve their performance, such that more stringent key performance indicators are met. These changes can be implemented at the UE side by utilizing sophisticated transmission schemes, multi-RAT support, or handover detection mechanisms [1], [4]–[6]. However, in most cases, a successful implementation of such advanced mechanisms requires the knowledge of the propagation channel that is subject to variations even for the static UE locations. Therefore, to facilitate the development of advanced transmission mechanisms allowing to optimize the delay in the conventional LPWANs, an in-depth understanding of the time-dependent propagation environment is essential.

This paper aims to provide a comprehensive analysis and develop robust models of the time-dependent propagation characterization for the NB-IoT technology. To this end, we conduct a long-term measurement campaign capturing the received signal characteristics of the stationary UE in rural and urban deployments including the reference signal receive power (RSRP) and signal-to-noise ratio (SNR). Further, we demonstrate that these characteristics are subject to drastic changes that affect the transmission performance of the UE. We then proceed with analyzing first- and second-order properties of these radio channel parameters. To capture them, we employ a doubly-stochastic Markov chain modeling framework. The model developed in this paper can be utilized as building block for analytical or simulation-based system-level studies of advanced mechanisms targeted at improving UE performance in LPWANs.

The main contributions of our study are the following.

- To support the performance optimization of existing LPWAN technologies, we conduct a long-term measurement

campaign by collecting the time-dependent statistical characteristics of the received signal in two representative deployments.
- Due to the importance of time-dependent radio dynamics, we offer free access to our measurement results from both urban and rural environments[1].
- Finally, to facilitate the development of advanced UE-side optimization solutions, we contruct a doubly-stochastic Markov model that captures both first- and second-order statistical properties of the received signal.

The rest of the paper is organized as follows. In Section II, we report on the measurement campaign and describe the setup of our experiments. A detailed study of the collected time-dependent statistics is provided in Section III. The developed models reflecting the time-dependent characteristics are presented in Section IV. Finally, the conclusions are drawn in the last section.

II. Measurement Campaign

As energy-limited sensors are expected to be in an operational state for many years, they may experience drastic differences in channel characteristics due to long-term changes in the environment, seasonal variations, etc. In this section, we describe our measurement campaign by introducing the considered scenarios, measurement equipment, and methodology.

TABLE I: Key parameters of LPWAN technologies [7]–[10].

	LoRaWAN	**Sigfox**	**NB-IoT**
Coverage (MCL)	157 dB	162 dB	164 dB
Technology	Proprietary (PHY), Open (MAC)	Proprietary	Open LTE
Spectrum	Unlicensed	Unlicensed	Licensed
Frequency	433, 868, 915 MHz	868, 915 MHz	700-2100 MHz
Bandwidth	125, 250, 500 kHz	100, 600 Hz	200 kHz
Max. ERP	14 dBm[2]	14 dBm[2]	23 dBm
Downlink data rate	0.3-50 kbps	0.6 kbps	0.5-27.2 kbps[1]
Uplink data rate	0.3-50 kbps	0.1-0.6 kbps	0.3-62.5 kbps[1]
Max. message size UL	242 B	12 B	1600 B
Max. message size DL	242 B	8 B	1600 B
Battery life	10+ years	10+ years	10+ years
Module cost	6 $	3 $	12 $
Security	AES-128	AES-128	LTE Security

[1] The value is release-dependent (Rel. 13).
[2] The value of max. ERP is relevant for the EU.

A. LPWAN Technology Selection

In this paper, we consider NB-IoT as a globally standardized LPWAN enabler. Today, it is arguably the most mature LPWAN technology publicly available worldwide [11].

As the NB-IoT operates over licensed spectrum, the network infrastructure is managed by supranational telecommunication companies, thus ensuring high availability and reliability. LoRaWAN infrastructure, on the other hand, is usually operated by local service providers. These companies may have difficulties to satisfy a service-level-agreement (SLA); hence, the LoRaWAN may not be used for critical infrastructure. The third well-known representative of LPWAN, Sigfox, provides similar guarantees as NB-IoT since all Sigfox networks are under the umbrella of the mother company. Therefore, Sigfox can assure the application SLA, but its technical parameters are not well-suited for data-intensive scenarios. Within the European region, the message size is limited by 12 B with 10 minutes period. This makes Sigfox unusable for application requiring more than 1728 B per day, see Table I for a more in-depth comparison of LPWAN technologies in question. From this perspective, NB-IoT represents the preferred candidate for most of the emerging mMTC scenarios [7], [9], [10].

[1]See https://github.com/martin146/globecom-2020

B. NB-IoT Technology

NB-IoT operates within the licensed LTE spectrum, which significantly reduces the interference from other technologies. On top of that, utilization of licensed bands does not impose any duty-cycle restrictions, and the maximum radiated power can be as high as 23 dBm. NB-IoT utilizes a reduced frequency band of 180 kHz, thus allowing for the deployment in a single LTE physical resource block (PRB). Further, it can operate in stand-alone mode (one global system for mobile communications (GSM) channel) or in the LTE guard band.

Uplink NB-IoT communication utilizes frequency division duplex (FDD) and single carrier-frequency division multiple access (SC-FDMA) with 15 or 3.75 kHz subcarrier spacing. The single-tone transmission uses binary phase-shift keying ($\pi/2$-BPSK) or quadrature phase-shift keying ($\pi/4$-QPSK) modulation. The highest throughput is achievable with multi-tone transmission relying on QPSK modulation with 15 kHz subcarrier spacing. In this case, the theoretical data-rate can be up to 62.5 kbps (in Rel. 14, up to 159 kbps) [7], [8].

One of the main benefits of NB-IoT is the prolonged battery life reaching 10 years. It is achieved mainly via the utilization of two power-saving mechanisms: (i) extended discontinuous reception (eDRX) and (ii) power-saving mode (PSM). The first mechanism allows the device to turn off its radio interface and receive messages only in pre-defined periodic intervals. The PSM provides even higher power savings by switching off the radio part entirely for a longer duration of up to 9920 hours [7].

C. Scenarios of Interest

For our measurement campaign, we considered both urban and rural communication use-cases. In the case of urban deployment, the sensor was placed on the rooftop of a Brno University of Technology (BUT) building. The sensor was positioned within 0.5 km distance from the nearest base station (BS). The rooftop placement significantly reduces the propagation impairments from dynamically moving obstacles, such as vehicles or pedestrians. Therefore, in these conditions, one may expect limited signal fluctuations over time.

The rural scenario includes a communication sensor placed in the cathodic protection test station located in South Bohemia, Czech Republic. The distance to the nearest BS was approximately 2 km. Due to that, we can expect reduced signal strength as compared to the urban scenario. As the sensor is placed only one meter above the ground, the signal quality can

be further degraded by the moving obstacles due to proximity of a district road.

D. Measurement Equipment

For both urban and rural measurements, we utilized identical types of sensors developed at BUT. The communication was ensured by the uBlox SARA-N210 NB-IoT module, which implements the technology according to LTE Rel. 13, i.e., Cat-NB1. It allows the module to utilize the maximum radiated power of 23 dBm. In combination with the 0 dBi half-wave dipole antenna, it offers the module the sensitivity of up to -135 dBm. As this version of the communication unit is primarily targeted for the European market, it supports only the frequency band of 800 MHz.

The sensors were equipped with Li-$SOCl_2$ cell to achieve the expected multi-year lifespan. These non-rechargeable batteries provide the highest specific capacity with self-discharge rate of only 1 % per year, and withstand high current peaks (around 300 mA) during the data transmissions [12].

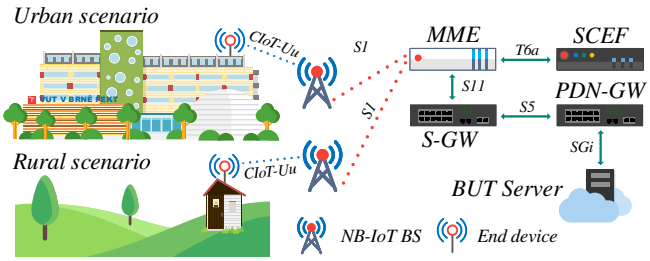

Fig. 1: Data flow in measurement scenarios.

From the perspective of the data flow, the communication bears significant resemblance to the traditional LTE, as depicted in Fig. 1. Data from the measuring device are wirelessly transmitted to the serving BS and routed through the evolved packet core (EPC) to the application server. In this case, we employed our application server at BUT premises. Since the main concern is the battery life-time, we utilized user datagram protocol (UDP), which adds only minimal overheads at the expense of reliability degradation.

E. Experiments and Data Collection

To achieve the required multi-year lifespan of the LPWAN sensors, only four messages were sent per day. This allowed us to observe changes in the radio environment with a 6-hour resolution. In the case of the rural area, the message period was extended up to 12 hours as worse radio and weather conditions were expected during the winter period. Particularly, temperatures below the freezing point negatively influence the battery performance.

To acquire a sufficient dataset displaying the time-dependent characteristics of the RSRP and SNR, we conducted a one-year-long measurement campaign. During this period, we obtained more than 1230 and 670 samples from urban and rural environments, respectively. Impressively, NB-IoT yields the success rate of more than 99.5 % for both scenarios. Such

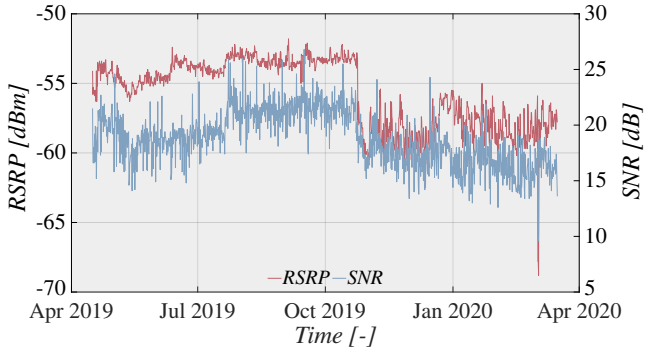

(a) Urban

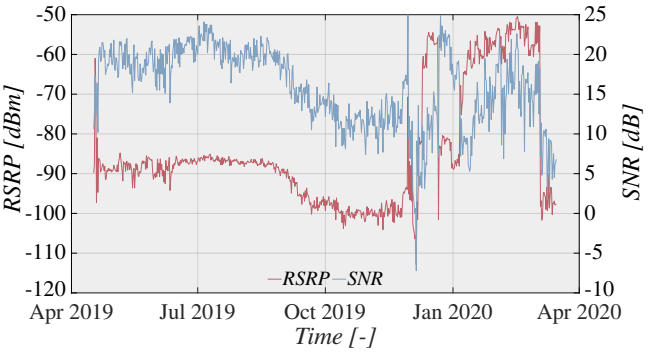

(b) Rural

Fig. 2: Time-dependent RSRP and SNR characteristics.

a high value can be explained by excellent average signal strength. For the sensor in an urban environment, the average value of RSRP does not fall below -56 dBm, see Fig. 2a. In the case of the rural sensor, RSRP oscillates around -90 dBm, and then slowly declines down to -100 dBm during the second third of the measurement period. The decreased signal levels, as compared to the urban deployment, were expected due to lower cell density. According to the study in [13], rural deployment is four-time sparser in contrast to the urban infrastructure, which is also verified by our measurements.

However, over the last third of the mesurement period, RSRP radically increases by approaching the urban values. A change in the network configuration, such as a new BS with better coverage, might have caused this difference. As a result, due to the required longevity of the LPWA sensors, all these events have to be taken into account. Accordingly, the prospective time-dependent model should also be able to capture these transitions.

III. Statistical Data Analysis

In this section, we characterize the time-dependent behavior of the RSRP experienced by the UE in the two considered propagation environments, urban and rural.

A. RSRP Time-Series

We proceed with statistical data analysis of the RSRP traces by keeping in mind the ultimate goal – simple yet accurate models. To preserve the trade-off between the mathematical

tractability and the accuracy of modeling, we search for an appropriate model in the class of covariance stationary ergodic stochastic processes. Recall that a stationary covariance process is fully characterized by the distribution of its single section and autocorrelation function (ACF) [14]. Therefore, to decide upon the choice of a suitable time-dependent model, we first need to assess the RSRP ergodic properties as well as estimate and analyze the first- and second-order characteristics of the RSRP process, i.e., the histogram of relative frequencies and the ACF of empirical data.

RSRP and SNR traces for both urban and rural environments are demonstrated in Fig. 2. There is a number of important conclusions to be drawn by visual analysis. First, there are indeed drastic variations in the propagation characteristics caused by environmental changes in both considered deployments. Second, one can clearly observe that it is possible to apply the notion of "hidden states" to the demonstrated behavior. Indeed, both SNR and RSRP shift their behavior between a set of so-called "levels" that are characterized by a long duration of samples oscillating around the mean value. Furthermore, the fluctuations within each level appear stochastically similar to the external observer. All these observations taken together support our primary hypothesis that the target model should clearly differentiate between the states, which have their unique stochastic properties.

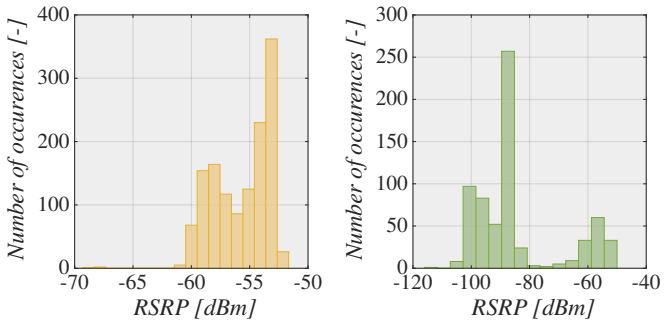

(a) Urban (b) Rural

Fig. 3: Histograms of relative frequencies.

B. First- and Second-Order Characteristics

The first-order characteristics of the RSRP stochastic process are represented by using the histograms of relative frequencies for both considered environments in Fig. 3. Here, one may notice that the histograms have multiple modes. Comparing this behavior to the measurement traces illustrated in Fig. 2, one may deduce that the observed peaks characterize the mean values of different states. This finding implies that our original hypothesis about state-based behavior is indeed confirmed.

The (normalized) ACF behavior representing the second-order properties of the propagation conditions is illustrated in Fig. 4 for both urban and rural environments including the respective confidence intervals. These boundaries are calculated

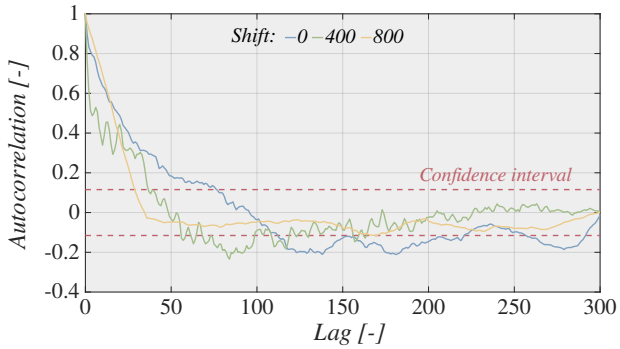

(a) Urban

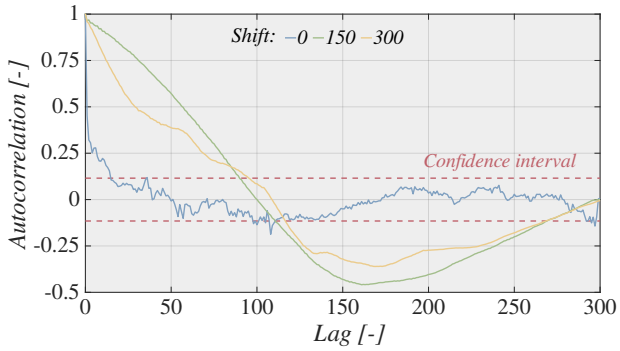

(b) Rural

Fig. 4: Autocorrelation functions of RSRP.

according to the rule of thumb [15] confirming the relation at lag i, i.e.,

$$|\overline{\rho_i}| \geq 2/\sqrt{n}, \tag{1}$$

where n is the lag and 2 represents an approximation of 1.96 in (1) corresponding to the confidence limit of $\alpha = 0.05$.

We specifically note that the ACF of empirical data is often prone to outliers and the initial point of the ACF estimation. Therefore, the only qualitative conclusions that can be safely made by observing the ACF are related to its structure, see, e.g., discussion in [16]. One such crucial conclusion is that the ACFs for both considered deployments are characterized by exponentially decaying behavior. This implies that the processes in question can be accurately modeled by using stochastic models with short-term memory.

C. Ergodicity and Stationarity

To verify whether the considered properties are, in fact, representative, we also need to test whether the considered processes are ergodic in nature. Recall that a sufficient condition of ergodicity is $K(n) \to \infty$, where $K(n)$ is n-lag ACF of the process. Observing Fig. 4, we may deduce that this condition does hold for both urban and rural deployments, thus implying that we may safely utilize the histogram, the relative frequencies, and the ACFs of a single trace as representative characteristics of the RSRP processes in the studied environments.

IV. Time-Dependent RSRP Modeling

In this section, we develop a time-dependent model for the statistical data reported in the previous section. Particularly, we show that the doubly-stochastic Markov chain framework is a convenient tool for characterizing the RSRP dynamics.

A. Doubly-Stochastic RSRP Modeling

Our analysis performed in the previous section suggests that the histogram of the relative frequencies is characterized by a generic shape, while the ACF has a distinct exponential decay. These properties are specific for the doubly-stochastic Markov chain models[2] that have been heavily utilized in the past for modeling traffic dynamics in packet networks, see, e.g., [18], [19]. Note that this type of models retains its analytical tractability and therefore can be used in both mathematical and simulation-based studies of LPWAN technologies [20].

There is a number of generic fitting algorithms developed for doubly-stochastic Markov models, such as those based on the expectation-minimization (EM) technique [21] or adaptation of maximum likelihood estimation [22]. However, these techniques are useful only when the internal structure is not clearly observable and/or the Markov modulating chain has a large number of states. In our case, one may resort to simpler techniques. To parameterize the doubly-stochastic Markov model, we need to determine the number of states, N, estimate the transition probabilities p_{ij}, $i, j = 1, 2, \ldots, N$ as well as the conditional probability mass functions (PMFs) associated with each state, $f_i(j)$, $i = 1, 2, \ldots, N$, $j \geq 0$.

To determine the number of states, N, in the modulating Markov chain, we apply kernel density estimation (KDE) to cluster the data [23], [24]. This process comprises two steps: (i) estimation of probability density function (PDF) and (ii) data clusterization based on the local maxima. The PDF of the samples is calculated as follows

$$\hat{f}(x) = \frac{1}{nh} \sum_{i=1}^{n} K\left(\frac{x - x_i}{h}\right), \tag{2}$$

where n is the sample size, h stands for the bandwidth, x is the actual value, and x_i represents the input samples. As a kernel smoothing function K, we used the PDF having a normal distribution. The bandwidth of the kernel smoothing function heavily impacts the resulting tightness of the approximation. In line with that, to obtain the optimally smoothed KDE, we calculate the bandwidth according to

$$h = \sigma \left(\frac{4}{3N}\right)^{1/5}, \tag{3}$$

where σ is the standard deviation and N is the sample size.

In the last step, the states of the Markov chain are derived from the local maxima of the resulting KDE. Each local maximum represents a single boundary of the Markov chain state. The two remaining edges are derived from the minimum and the maximum RSRP values of the input data set.

[2]These models are also known as hidden Markov chains [17].

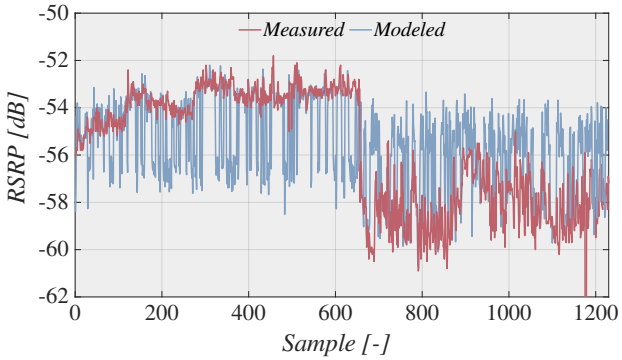

(a) Urban

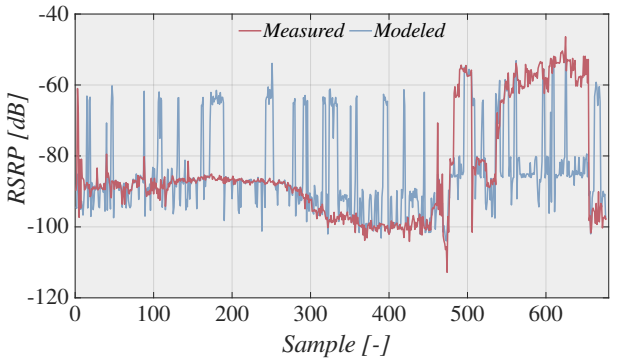

(b) Rural

Fig. 5: Comparison of RSRP traces.

Once the number of states N is established, we proceed to determine the transition probabilities p_{ij}, $i, j = 1, 2, \ldots, N$ and PMFs associated with each state, $f_i(j)$, $i = 1, 2, \ldots, N$, $j \geq 0$ by using the conventional statistical methodologies. We first define the state boundaries between the states and then calculate the number of state changes for the particular values of i and j between the previous and the current value in the trace and divide it by the number of samples in the trace size.

B. Numerical Assessment

We further proceeded by analyzing the results of the proposed doubly-stochastic Markov chain modeling for both urban and rural scenarios. To this aim, Fig. 5 demonstrates a visual comparison of empirical and generated RSRP traces. As one may observe, the main "state-based" nature of the empirical traces is adequately captured by our model. It must be noted that the developed model is based on a Markov chain, which is, by nature, memoryless. Therefore, it is not possible to precisely follow the input data sequence. The decision as to which state to depart from is not determined by the previous state but only by the current one. The future state, therefore, relies solely on the probabilities of the transition matrix for a particular state.

A comparison of histograms of the relative frequencies is provided in Fig. 6. Here, on top of the visual comparison, we also performed χ^2 statistical test for the heterogeneity of the samples. With the level of significance $\alpha = 0.05$, the test

shows that both samples belong to the same distribution for both considered environments.

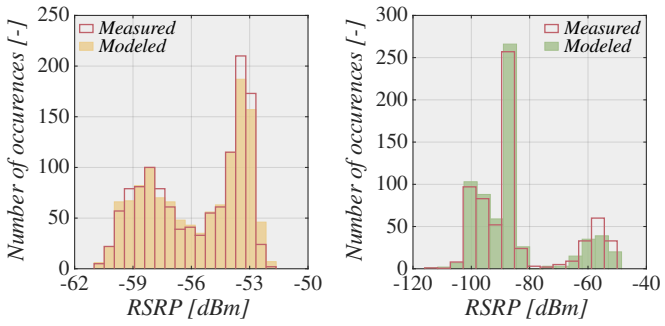

(a) Urban (b) Rural

Fig. 6: Histograms of relative frequencies forour model.

A comparison of ACFs is provided in Fig. 7. As expected, there is no perfect match for the ACFs, as they are heavily impacted by the initial estimation point. Nevertheless, our doubly-stochastic Markov model adequately captures the short-memory of the process. To confirm this visual observation, we have also performed a Box-Ljung statistical test for the correlation of the first M lags [25]. The test shows that for the empirical and the generated traces in both environments, there is a statistically confirmed correlation up to the lag $n = 10$.

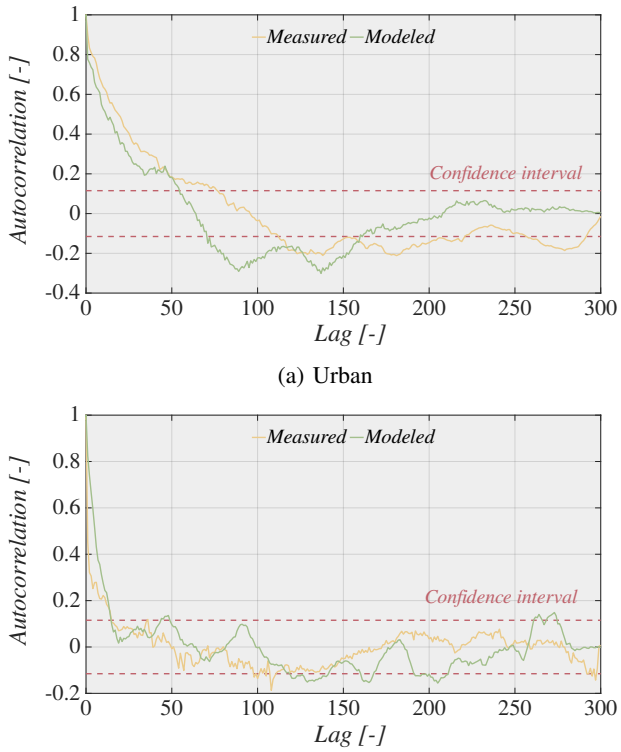

(a) Urban

(b) Rural

Fig. 7: Comparison of autocorrelation functions.

V. Conclusions

The research reported in this paper is mainly motivated by the ongoing attempts to optimize modern LPWAN technologies and adapt them to the needs of novel IoT applications and services that are more sensitive to delays and losses. Accordingly, we first report the results of our long-term NB-IoT measurement campaign of RSRP dynamics in two representative propagation environments, rural and urban. Our statistical analysis illustrates that in both considered environments, the RSRP perceived by a stationary UE is subject to drastic fluctuations at small and large scales, thus leading to a complex structure of the RSRP stochastic process.

We further study the distributional and correlational properties of the RSRP process. Then, we demonstrate that these properties may be tightly captured by utilizing a doubly-stochastic Markov chain framework. Parameters of the particular models for the considered environments are also reported and can be used as reference cases. The reported models retain analytical tractability, thus allowing for further studies and optimization of modern LPWAN technologies. They can be used for generating sufficiently long traces in case the input data set is not extensive enough. Their potential applicability falls within the reinforcement learning area, where a relatively long input data sequence (tens of thousands of samples) is needed to generate a sufficiently accurate model. Using the introduced method, it is possible to extend a shorter input sequence (e.g., less than 700 values) as required.

Acknowledgment

For this research, the infrastructure of the SIX Center was used. This research was financed by the Ministry of Industry and Trade of the Czech Republic, project no. FV40371. Tampere University work was supported by the Business Finland Project 5G-FORCE.

References

[1] S. K. Sharma and X. Wang, "Toward Massive Machine Type Communications in Ultra-Dense Cellular IoT Networks: Current Issues and Machine Learning-Assisted Solutions," *IEEE Communications Surveys & Tutorials*, vol. 22, no. 1, pp. 426–471, 2020.

[2] International Telecommunication Union, "Guidelines for Evaluation of Radio Interface Technologies for IMT-2020," ITU-R, Report ITU-R M.2412-0, October 2017.

[3] A. Mukherjee, *5G New Radio: Beyond Mobile Broadband*. Artech House, 2019. [Online]. Available: https://books.google.cz/books?id=X7jEDwAAQBAJ

[4] S. Kavuri, D. Moltchanov, A. Ometov, S. Andreev, and Y. Koucheryavy, "Performance Analysis of Onshore NB-IoT for Container Tracking During Near-the-Shore Vessel Navigation," *IEEE Internet of Things Journal*, vol. 7, no. 4, pp. 2928–2943, 2020.

[5] K. Mikhaylov, V. Petrov, R. Gupta, M. A. Lema, O. Galinina, S. Andreev, Y. Koucheryavy, M. Valkama, A. Pouttu, and M. Dohler, "Energy Efficiency of Multi-Radio Massive Machine-Type Communication (MR-MMTC): Applications, Challenges, and Solutions," *IEEE Communications Magazine*, vol. 57, no. 6, pp. 100–106, 2019.

[6] V. Petrov, A. Samuylov, V. Begishev, D. Moltchanov, S. Andreev, K. Samouylov, and Y. Koucheryavy, "Vehicle-based Relay Assistance for Opportunistic Crowdsensing over Narrowband IoT (NB-IoT)," *IEEE Internet of Things journal*, vol. 5, no. 5, pp. 3710–3723, 2017.

[7] O. Liberg, *Cellular Internet of Things*, 1st ed. Cambridge: Elsevier, 2019.

[8] A. Hoglund, X. Lin, O. Liberg, A. Behravan, E. A. Yavuz, M. Van Der Zee, Y. Sui, T. Tirronen, A. Ratilainen, and D. Eriksson, "Overview of 3GPP Release 14 Enhanced NB-IoT," *IEEE Network*, vol. 31, no. 6, pp. 16–22, November 2017.

[9] Sigfox, "Sigfox Connected Objects: Radio Specifications," Sigfox, Ref.: EP-SPECS, Rev.: 1.4, November 2019.

[10] LoRa Alliance™, "LoRaWAN™ 1.1 Specification," LoRa Alliance™, Final release, October 2017.

[11] L. Feltrin, G. Tsoukaneri, M. Condoluci, C. Buratti, T. Mahmoodi, M. Dohler, and R. Verdone, "Narrowband IoT: A Survey on Downlink and Uplink Perspectives," *IEEE Wireless Communications*, vol. 26, no. 1, pp. 78–86, 2019.

[12] P. Masek, M. Stusek, K. Zeman, J. Hosek, K. Mikhaylov, S. Andreev, Y. Koucheryavy, O. Zeman, J. Votapek, and M. Roubicek, "Tailoring NB-IoT for Mass Market Applications: A Mobile Operator's Perspective," in *2018 IEEE Globecom Workshops (GC Wkshps)*, 2018, pp. 1–7.

[13] M. Lauridsen, H. Nguyen, B. Vejlgaard, I. Z. Kovacs, P. Mogensen, and M. Sorensen, "Coverage Comparison of GPRS, NB-IoT, LoRa, and SigFox in a 7800 km^2 Area," in *2017 IEEE 85th Vehicular Technology Conference (VTC Spring)*, June 2017, pp. 1–5.

[14] S. Karlin, *A First Course in Stochastic Processes*. Elsevier Science, 2014.

[15] T. C. Krehbiel, "Correlation Coefficient Rule of Thumb," *Decision Sciences Journal of Innovative Education*, vol. 2, no. 1, pp. 97–100, 2004. [Online]. Available: https://onlinelibrary.wiley.com/doi/abs/10.1111/j.0011-7315.2004.00025.x

[16] A. Dürre, R. Fried, and T. Liboschik, "Robust Estimation of (Partial) Autocorrelation," *Wiley Interdisciplinary Reviews: Computational Statistics*, vol. 7, no. 3, pp. 205–222, 2015.

[17] L. Rabiner and B. Juang, "An Introduction to Hidden Markov Models," *IEEE ASSP Magazine*, vol. 3, no. 1, pp. 4–16, 1986.

[18] S. B. Slimane and T. Le-Ngoc, "A Doubly Stochastic Poisson Model for Self-Similar Traffic," in *Proceedings IEEE International Conference on Communications ICC'95*, vol. 1. IEEE, 1995, pp. 456–460.

[19] D. Moltchanov, Y. Koucheryavy, and J. Harju, "The Model of Single Smoothed MPEG Traffic Source Based on the D-BMAP Arrival Process with Limited State Space," in *Proceedings of ICACT*, 2003, pp. 55–60.

[20] A. Ometov, D. Moltchanov, M. Komarov, S. V. Volvenko, and Y. Koucheryavy, "Packet Level Performance Assessment of mmWave Backhauling Technology for 3GPP NR Systems," *IEEE Access*, vol. 7, pp. 9860–9871, 2019.

[21] W. Khreich, E. Granger, A. Miri, and R. Sabourin, "A survey of Techniques for Incremental Learning of HMM Parameters," *Information Sciences*, vol. 197, pp. 105–130, 2012.

[22] M. J. Gales, "Maximum Likelihood Linear Transformations for HMM-Based Speech Recognition," *Computer Speech & Language*, vol. 12, no. 2, pp. 75–98, 1998.

[23] Y. Huang, X. Chen, and W. B. Wu, "Recursive Nonparametric Estimation for Time Series," *IEEE Transactions on Information Theory*, vol. 60, no. 2, pp. 1301–1312, Feb 2014.

[24] A. Hinneburg and D. A. Keim, "A General Approach to Clustering in Large Databases with Noise," *Knowledge and Information Systems*, vol. 5, no. 4, pp. 387–415, 2003. [Online]. Available: https://doi.org/10.1007/s10115-003-0086-9

[25] P. Burns, "Robustness of the Ljung-Box Test and Its Rank Equivalent," *Available at SSRN 443560*, 2002.